J Mater Sci (2010) 45:3833–3840
DOI 10.1007/s10853-010-4438-z

Physiochemical characterizations of electrospun ($ZnO–GeO_2$) nanofibers and their optical properties

Muzafar A. Kanjwal · Nasser A. M. Barakat · Faheem A. Sheikh · Dae Kwang Park · Hak Yong Kim

Received: 21 December 2009 / Accepted: 23 March 2010 / Published online: 6 April 2010

Abstract In this study, nanofiber mats consisting of two potential metal oxides were produced by electrospinning technique. An aqueous solution of zinc acetate dihydrate and germanium isopropoxide was mixed with polyvinyl alcohol solution to prepare a sol–gel that was electrospun at 20 kV. The obtained nanofiber mats were dried under a vacuum at 80 °C for 24 h and then calcined in air at different temperatures and soaking times. Physiochemical characterizations have affirmed that nanofibers composed of zinc oxide-germanium dioxide ($ZnO–GeO_2$) can be prepared by calcination at different temperatures. Scanning electron microscopy (SEM), transmission electron microscopy (TEM), and the Brunauer–Emmett–Teller (BET) technique were employed to characterize the as-spun nanofibers and the calcined product. The specific surface area of the calcined product decreased with increases in temperature. X-ray powder diffractometery (XRD) analysis was used to study the chemical composition and the crystallographic structure. The optical properties of the as-prepared $ZnO–GeO_2$ nanofibers were also studied.

M. A. Kanjwal
Department of Polymer Nano Science and Technology, Chonbuk National University, Jeonju 561-756, Republic of Korea

N. A. M. Barakat
Chemical Engineering Department, Faculty of Engineering, El-Minia University, El-Minia, Egypt

N. A. M. Barakat (✉) · F. A. Sheikh
Bionano System Engineering, Chonbuk National University, Jeonju 561-756, Republic of Korea
e-mail: nasbarakat@yahoo.com

D. K. Park · H. Y. Kim (✉)
Department of Textile Engineering, Chonbuk National University, Jeonju 561-756, Republic of Korea
e-mail: khy@chonbuk.ac.kr; kanjwalmuzafar@gmail.com

Introduction

One-dimensional (1D) nanomaterials, including nanotubes, nanorods, nanowires, nanobelts, and nanofibers, show some distinctive properties compared with other nanoparticles. Among these 1D nanostructures, nanobelts and nanofibers are of especial interest due to their high surface area-to-volume ratio [1]. Single oxide nanofibers or nanobelts have been synthesized by many researchers. However, single oxides have limited electrochemical properties. To produce 1D nanostructures with novel physical and chemical properties, some researchers have investigated the synthesis of nanostructures consisting of two oxides [2–9].

In this study, we describe the synthesis of nanofibers composed of a mixture of two functional oxides ($ZnO–GeO_2$) and their optical properties. Due to its intrinsic defects and its superior conducting properties, Zinc oxide (ZnO) has been investigated as a piezoelectric material and a transparent conducting material for fabricating solar cells, sensors, and electrodes [10]. ZnO is a versatile material with applications in compound semiconductors, photoelectronics, electronics, and catalysis [11]. It is a thermally and chemically stable *n*-type semiconductor material with a well-known wide band gap of 3.37 eV and a high-exciton-binding energy of 60 mV at room temperature. ZnO had been frequently doped with group III and VII elements to enhance the electrical properties [12].

Germanium is a semiconductor transition metal used in optical devices, radiation detectors, and electronic industry [13]. Germanium nanostructures have high hole and electron mobilities. Compared to silicon (4.9 nm), germanium nanostructures have a larger exciton radius of 24.3 nm and, therefore, show more quantum effects [14, 15]. It is worth mentioning that the use of complementary metal oxide semiconductors (CMOS) has increased interest in this

material [16]. Ge is an indirect band gap semiconductor material with a smaller energy difference between the direct gap and the indirect gap ($\Delta E = 0.12$ eV). Moreover, the ionic radius difference between a Zn ion (0.74 Å) and a Ge ion (0.53 Å) is small. These properties indicate that it should be much easier to tune the electronic properties around the band edge [17]. Yu et al. [18] recently reported the preparation of ZnO:Ge by the solid state reaction process and examined its optical properties. They observed that a Zn_2GeO_4 phase was formed by the doping of Ge atoms and attributed the luminescence center to the basic effects of ZnO and the contamination effects of GeO_2. These materials have excellent applications as oxide phosphors in optoelectronics [19]. Germanium dioxide (GeO_2) is a wide band gap material with several optical properties of interest in the field of optoelectronics and is known to influence the properties of products [20]. The emission at room-temperature of the products can be attributed to the Ge–O vacancies and the singly ionized oxygen vacancies. ZnO/GeO_2 nanomaterials with excellent optical properties and in various shapes such as core–shell, multipods, etc., have been reported by different research groups [20, 21]. The novel synthesis of ZnO coupled GeO_2 nanofibers, and the determination of their optical properties has not been reported in the literature.

In this study, we describe the synthesis of nanofibers composed of a mixture of two functional oxides (ZnO–GeO_2). Smooth, continuous ZnO–GeO_2 nanofibers have been prepared by electrospinning. Electrospinning is a facile technique employed to create high surface area-to-volume fibers. Electrospun fibers have diameters ranging from tens of nanometers to several micrometers, orders of magnitude smaller than those produced by conventional spinning techniques [22–24], and approximately double the surface area of continuous thin films [25].

Experimental section

Materials

Zinc acetate dihydrate assay (99.0%) was obtained from Showa, Co. Japan. Poly vinyl alcohol (PVA) with a molecular weight (MW) of 65,000 g/mol was obtained from Dong Yang Chem. Co., South Korea. Germanium (1 V) isopropoxide (97%) was obtained from Aldrich USA. These materials were used without any further purification. Distilled water was used as the solvent.

Characterization

The surface morphology of nanofibers was studied using a JEOL JSM-5900 scanning electron microscope, JEOL Ltd., Japan. The surface area of the nanofibers was measured using the Brunauer–Emmett–Teller (BET) technique (ASAP 2010 micromeritics, USA). The phase and crystallinity were characterized using a Rigaku X-ray diffractometer (Rigaku Co, Japan) with Cu Kα ($\lambda = 1.54056$ Å) radiation over a 2θ range from 20 to 90°. Before TEM analysis, the powdered samples were dispersed in methanol by sonication, placed on a copper grid covered with holey carbon film, and dried by normal evaporation. High-resolution images and selected area electron diffraction patterns were observed using a JEOL JEM 2010 transmission electron microscope (TEM) operating at 200 kV, JEOL Ltd., Japan. Thermal gravimetric analysis was performed with a Pyris1 TGA analyzer, Perkin Elmer Inc, USA. The surface composition was determined by X-ray photoelectron spectroscopy analysis (XPS, AXIS-NOVA, Kratos Analytical Ltd, UK) using the following conditions: base pressure 6.5×10^{-9} Torr, resolution (pass energy) 20 eV, and scan step 0.05 eV/step. The optical properties were studied using HP 8453 UV Visible Spectroscopy System; spectra obtained were analyzed by HP ChemiStation software 5890 series. Additionally, the quantum effect of nanofibers was investigated by photoluminescence (PL) spectrum of ZnO–GeO_2 nanofibers measured with a He–Cd laser at room temperature under 325 nm (3.82 eV) ultraviolet light excitation and a filter wavelength of 355 nm.

Electrospinning setup

An aqueous metal acetate/isopropoxide solution was prepared by dissolving zinc acetate (ZnAc) and germanium isopropoxide (GeIsp) in water at a ratio of 1:0.5:4. A sol–gel was prepared by mixing the obtained solution with a PVA aqueous solution (10 wt%) at a ratio of 5.5:20. Typically, 1 g of ZnAc and 0.5 g of GeIsp were dissolved in 4 g of water and then mixed with 20 g of the PVA solution (10 wt%). The mixture was vigorously stirred at 50 °C for 5 h. The sol–gel was supplied through a plastic syringe attached to a capillary tip. A copper wire originating from the positive electrode (anode) was inserted into the sol–gel, and a negative electrode (cathode) was attached to a metallic collector covered with a polyethylene sheet. A voltage of 20 kV was applied to the solution. The formed nanofiber mats were initially dried for 24 h at 80 °C under a vacuum and then calcined at different temperatures for 1 h in air with a heating rate of 2 °C/min. Figure 1 shows a conceptual schematic illustration for the electrospinning setup used. A high voltage power supply (CPS-60 K02V1, Chungpa EMT Co., Republic of Korea) was used as the source of the electric field [26].

Results and discussion

Electrospinning is a fascinating technique that involves the use of a high voltage to charge the surface of a droplet of

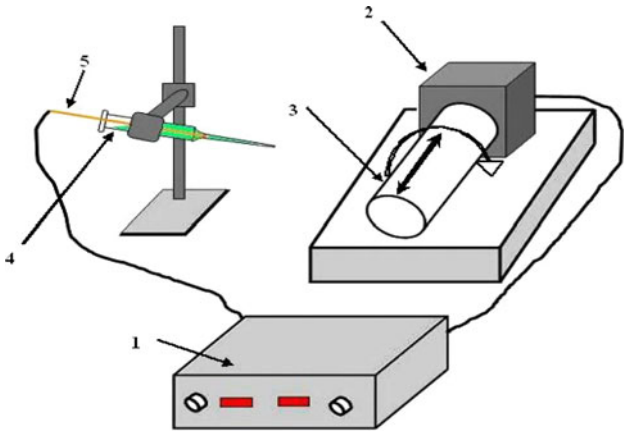

Fig. 1 Schematic diagram of a simple electrospinning apparatus: (1) dc power supply (2) Electric motor (3) Rotating collector (4) Syringe (5) Copper tip

polymer solution, to induce the ejection of a liquid jet through a spinneret. The jet is consequently stretched many times to form smooth, continuous, ultrathin fibers [27]. Figure 2 shows the ZnAc/GeIs/PVA nanofiber mats after drying. As shown in the low-magnification image in Fig. 2a, the obtained mats are bead-free and composed of separated nanofibers. The mixing of ZnAc and GeIsp does not affect the efficiency of the electrospinning process. In other words, the electrospinning of the prepared sol–gel produced smooth and continuous nanofibers 2B.

Calcination of the vacuum-dried ZnAc/GeIs/PVA nanofiber mats in an oxygen atmosphere affected the morphology of the nanofibers. Panels a and b of Fig. 3 depict low- and high-magnification SEM images after calcination of ZnAc/GeIs/PVA nanofibers at 600 °C. As shown in these images, calcination at 600 °C was not adequate to obtain nanofibers with good morphology. In other words, a higher temperature is required to enhance the densification of the nanofibers. Figure 3 shows the low- and high-magnification SEM images for nanofibers produced at calcination temperatures of 700 °C (panels c and d) and 800 °C (panels e and f). These figures indicate that increasing the calcination temperature improved the nanofiber morphology. These results suggest that the optimum calcination temperature is 700 °C. As shown in panels c and d of Fig. 3, the nanofibers calcined at 700 °C do not have defects. Increasing the calcination temperature deformed the nanofibers by producing protrusions on the surface of the nanofibers. At a relatively low calcination temperature (600 °C), the nanofibers were solid, semi-smooth, and possessed some defacements (Fig. 3, panels a and b).

XRD is a reliable technique for investigating the nature of any crystalline material. Figure 4 shows the XRD patterns of the nanofibers after calcination of ZnAc/GeIs/PVA nanofiber mats at 600–800 °C. Calcination of ZnAc/GeIs/PVA nanofiber mats at high temperatures completely eliminated the PVA polymer and resulted in the formation of zinc oxide and germanium dioxide. As shown in the spectra in Fig. 4a, the existence of strong diffraction peaks at 2θ values of 20.94° and 25.94°, and other peaks at increasing temperatures of 37.91°, 44.01°, 53.05°, 57.82°, 65.84°, and 67.23° correspond to the crystal planes (100), (101), (102), (201), (202), (211), (203), and (301), respectively, and indicate the formation of the germanium dioxide [JCPDS card no 36-1463]. In addition to these peaks, the apparent peaks at 2θ values of 31.76°, 34.42°, 36.25°, 47.76°, 56.61°, 62.86°, and 67.92° correspond to the crystal planes of (100), (002), (101), (102), (110), (103), and (112), confirming the formation of pure zinc oxide (JCPDS card No 36-1451). The XRD spectra of Fig. 4b and c calcined at 700 to 800 °C are similar to Fig. 4a. They exactly match the standard spectrum of zinc oxide and germanium dioxide, though the intensity of the peaks increased with increasing temperature. To simplify Fig. 4 we have marked the peaks corresponding to germanium dioxide and zinc oxide as Ge and Z, respectively. Overall, the XRD results confirm the formation of ZnO–GeO_2 nanofibers.

Thermo-gravimetric analysis (TGA) in air was employed to explain the mechanism of (ZnO–GeO_2) nanofiber formation from ZnAc/GeIs/PVA electrospun mats. Figure 5 shows the obtained TGA results, along with the first

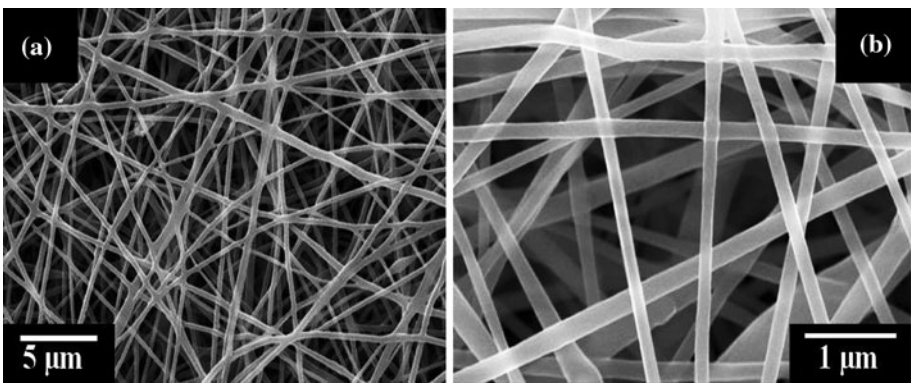

Fig. 2 Scanning electron microscope (SEM) images for the dried ZnAc/GeIs/PVA nanofibers in low (**a**) and high magnification (**b**)

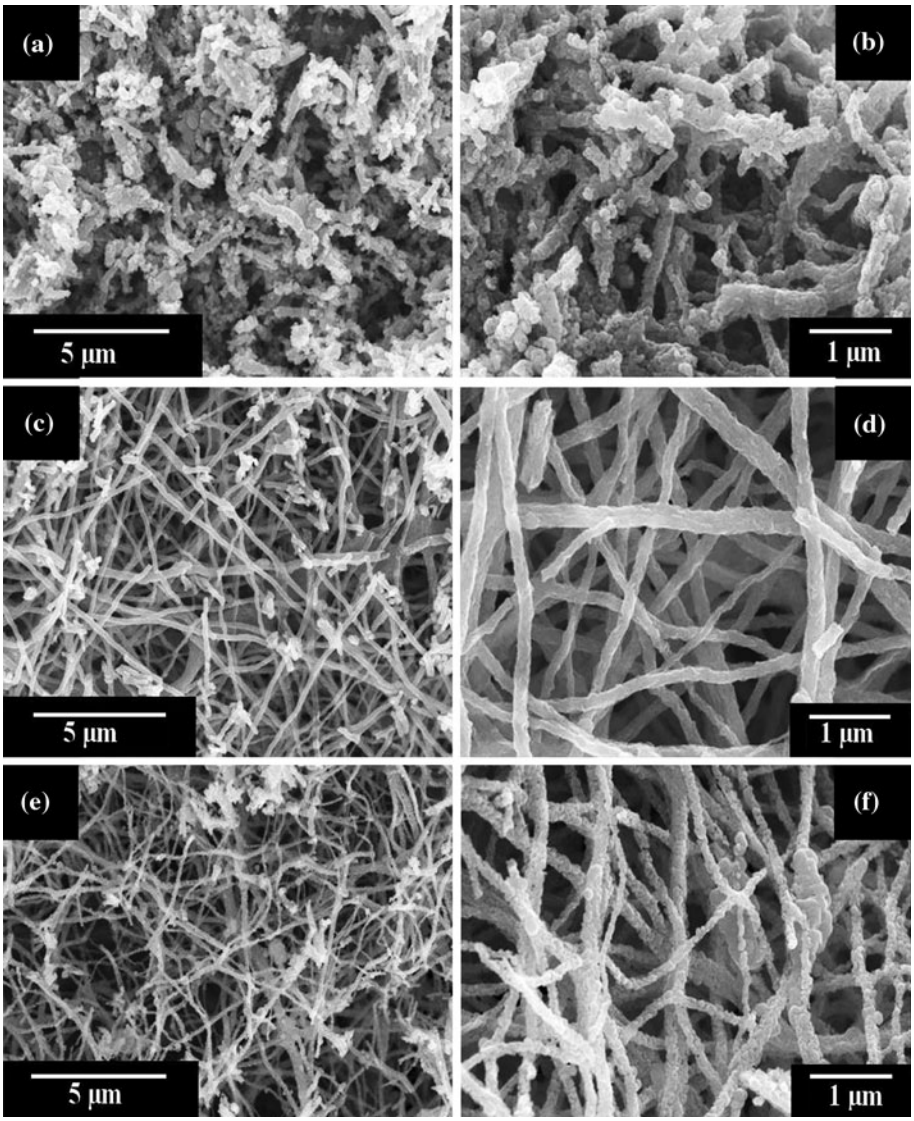

Fig. 3 Low- and high-magnification SEM images obtained after calcination of the ZnAc/GeIs/PVA nanofiber mats at 600 (**a** and **b**), 700 (**c** and **d**), 800 °C (**e** and **f**) for 1 h

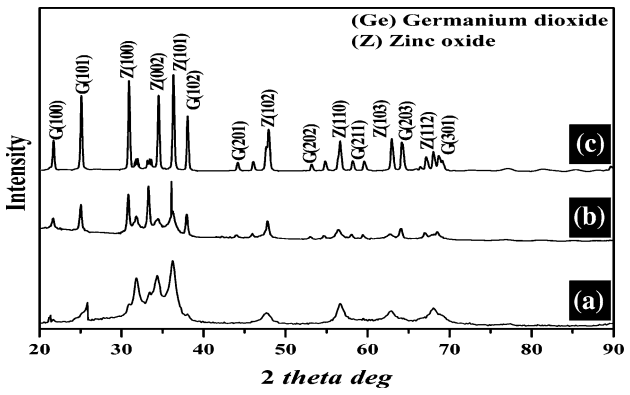

Fig. 4 XRD data for the nanofibers after calcination of the ZnAc/GeIs/PVA nanofiber mats at 600 (**a**), 700 (**b**), 800 °C (**c**) for 1 h. The crystal planes corresponding to the observed peaks are identified

derivatives curve. Below 100 °C, anhydrous zinc acetate is first formed with the crystallization water removed from Zn $(CH_3COO)_2{\cdot}2H_2O$ under a continuous flow of dry air. The anhydrous zinc acetate begins to decompose into ZnO at ~125 °C, and the decomposition process, accompanied by an exothermic reaction, is nearly complete at ~250 °C [28]. The total weight loss is about 40%. In this temperature range, PVA is also eliminated at ~245 °C [29]. Figure 5 also shows significant weight loss between 250 and 570 °C. In this temperature range, germanium isopropoxide might be decomposed to germanium dioxide. As there is no major weight loss above 570 °C [30], indicating the formation of pure inorganic oxide, the calcination temperature should be above 570 °C.

The inner structure of the synthesized ZnO–GeO_2 nanofibers was studied by transmission electron microscopy

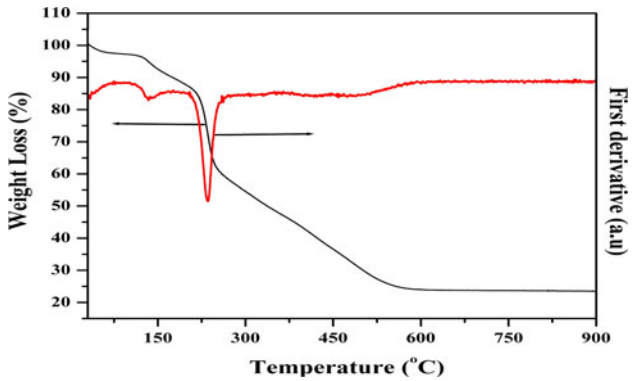

Fig. 5 Thermo-gravimetric analysis in oxygen atmosphere for the electrospun ZnAc/GeIs/PVA nanofibers, along with the first derivative of the ZnAc/GeIs/PVA data

(TEM), high-resolution transmission electron microscopy (HRTEM), and selected area electron diffraction pattern (SAED) analysis. Figure 6a shows a TEM image of calcined nanofibers at 600 °C that resembles the SEM images in morphology, dimensions, and density. An HRTEM image of the edge of a synthesized nanofiber is depicted in Fig. 6b. As shown, the atomic planes are not uniformly arranged in a parallel manner, indicating poor crystallinity preventing the identification of the atomic planes. The SAED pattern in the inset of Fig. 6b also reveals an unsatisfactory crystalline structure. Increasing the calcination temperature enhanced the crystallinity of the $ZnO–GeO_2$ nanofibers, as shown in Fig. 6. The TEM and HRTEM images along with the SAED patterns of the nanofibers are shown in panels c and d for

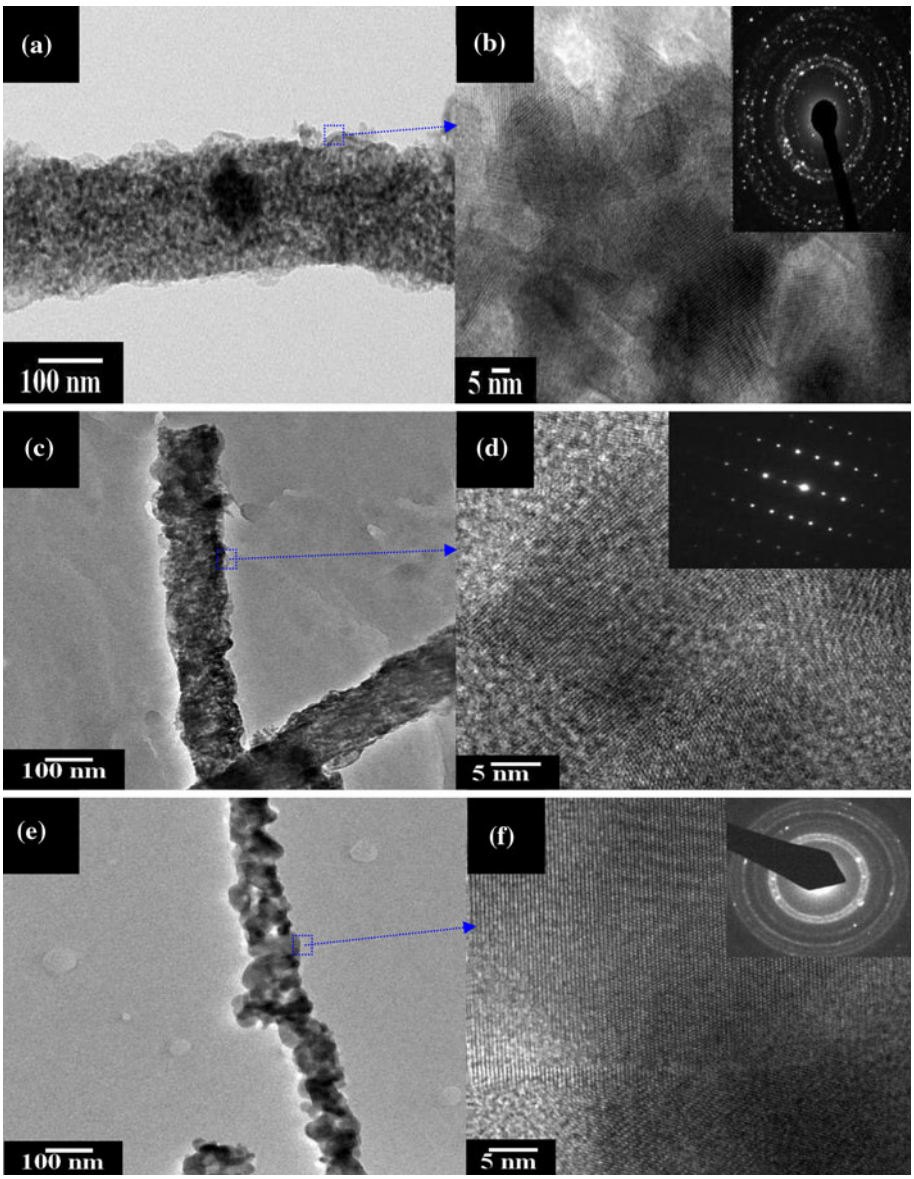

Fig. 6 TEM image and HRTEM image at the nanofiber edge for a $ZnO–GeO_2$ nanofibers along with corresponding SAED pattern for the marked area at 600 (**a** and **b**), 700 (**c** and **d**) and 800 °C (**e** and **f**) for 1 h

Table 1 Band gap energies, BET surface areas, and grain sizes at different temperatures of the ZnO–GeO_2 nanofibers

(ZnO–GeO_2) nanofibers at different temperatures	E photon (eV)	BET surface area (m^2/g)	Grain size (nm)
600 °C	(1.59), (2.83), (4.40)	137.8478	7
700 °C	(2.01), (3.25), (4.61)	45.419	8
800 °C	(2.52), (3.65), (4.71)	34.585	17

nanofibers produced at 700 °C and in panels e and f for nanofibers calcined at 800 °C. Figure 6d shows confirmation that the atomic planes are parallel and are arranged in an orderly geometry, confirming that the optimum calcination temperature was 700 °C. Moreover, the SAED image demonstrates excellent crystallinity. It is important to note that the grain size increases linearly with increase in temperatures, as displayed in Table 1.

To investigate the effect of calcination temperature on the surface area of the produced nanofibers, the BET technique (ASAP 2010 micromeritics, USA) was utilized. The obtained results agreed with the TEM images. The average surface area of the calcined nanofibers decreases linearly with increasing temperature, as shown in Table 1.

To investigate the oxidation states and possible changes of binding energies in the synthesized ZnO–GeO_2 nanofibers, X-ray photoelectron spectroscopy (XPS) analysis was performed. The samples used in XPS, were supported on carbon cloth electrodes, as widely used in electrochemical experiments. No heat treatment on the samples was needed. The results are shown in Fig. 7. The peak at 283.82 eV corresponding to C 1 s is due to the graphite tape used during the sampling process. The Zn 2p region in ZnO mostly consists of 2p1/2 and 2p3/2 spin–orbit components at binding energies of 1042 eV and 1019 eV, respectively. In addition to 2p, we also observed 3d, 3p and 3 s spin–orbit components for Zn at the binding energies of 8 eV, 86.48 eV and 138 eV, respectively [31]. Similarly, the Ge 3d region in germanium dioxide shown in the inset consists of Ge 3d3/2 spin–orbit components at binding energies of 29 eV [32]. The O 1 s peak for oxygen is easily identified at the binding energy of 529 eV.

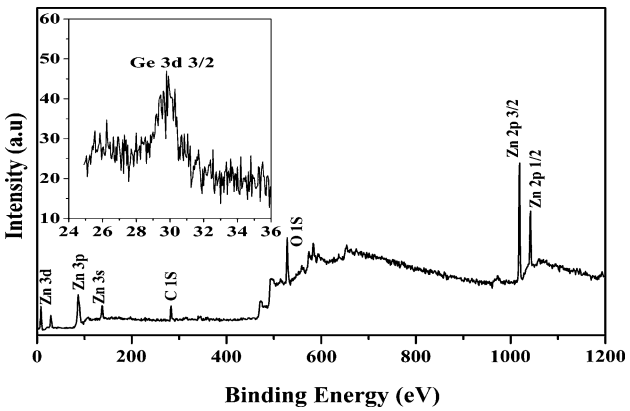

Fig. 7 XPS results for the nanofibers after the calcination process. The inset shows the Ge 3D region with a low scan rate (29 eV)

Photoluminescence study

Figure 8a shows the absorbance spectra for the synthesized nanofibers at different temperatures. Two sharp peaks can be observed at 207 and 379 nm that, may be attributed to two different materials (germanium dioxide and zinc oxide). Figure 8b shows the room temperature PL spectra for the ZnO–GeO_2 nanofibers synthesized at temperatures of 600, 700, and 800 °C. PL properties are dependent on the process parameters such as atmosphere, substrate temperature, reaction time, etc. To improve the PL intensity of the synthesized nanofibers, the samples were calcined in an oxygen atmosphere at different temperatures. The observed emission behavior is very different from the

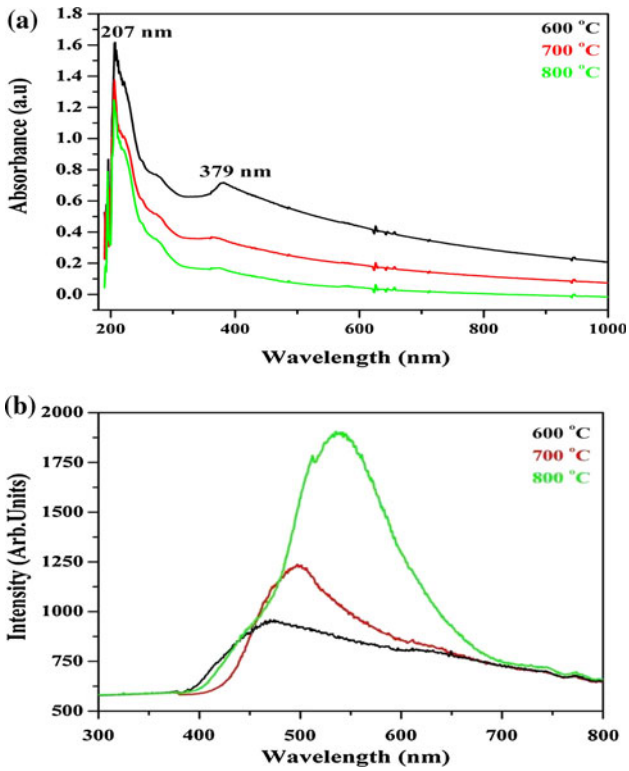

Fig. 8 UV–visible spectra for the ZnO–GeO_2 nanofibers at different temperatures (**a**). Room temperature PL spectra for the nanofibers after calcination of the ZnAc/GeIs/PVA nanofiber mats at different temperatures for 1 h (**b**)

classical band-gap emission of undoped zinc oxide. The intensity of the luminescence band in the visible spectral range increases with increased temperature. To our knowledge, the red shift from 475 to 540 nm with increased temperature in ZnO–GeO_2 nanofibers has never been reported. The UV emission, known as near-band-edge emission (NBE) originates from the recombination of free-excitons through an exciton–exciton collision process. The green emission is due to the recombination of a photo-generated hole with an electron occupying an oxygen vacancy. [33, 34]. Both near-band-edge emission and green emission depend significantly on the preparation methods and conditions [35]. Therefore, the appearance of sharp, strong intensity green emissions and no NBE emissions indicate that ZnO–GeO_2 nanofibers have various intrinsic defects in the ZnO and Ge crystals. Enhancement of the green emission in ZnO–GeO_2 nanofibers might be of interest for typical applications, such as field emissive display technology, etc.

Optical band gap

For semiconductor materials, the quantum confinement effect is expected if the semiconductor dimension is smaller than the Bohr radius of the excited state and the absorption edge is shifted to a higher energy [36–38]. For a semiconductor, the absorbance in the vicinity of the onset due to the electronic transition is given by

$$\alpha = \frac{K\left(h\nu - E_g\right)^n}{h\nu}$$

where α is the absorption coefficient, K is a constant, E_g is the band gap, and n is a value that depends on the nature of the transition (1/2 for a direct allowed transition or 2 for an indirect allowed transition) [39, 40]. As this case deals with direct allowed transitions, n is equal to 1/2. The band gap can be estimated from a plot of photon energy versus $(\alpha h\upsilon)^2$. For ZnO–GeO_2 nanofibers, three band gap energies can be detected at each temperature, as shown in Fig. 9 and Table 1. The linear regions in this plot can be used to estimate the band gap energies by calculating the intersection points between these regions and the abscissa (x-axis). The nanofibrous morphology enhances the optical properties of the nanostructure [41]. Extrapolation of the linear regions in the graph gives the E_g value for these formulations.

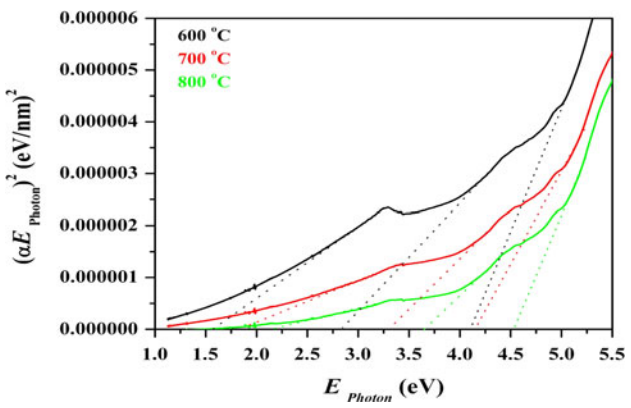

Fig. 9 Plot of $(\alpha E_{\text{Photon}})^2$ versus E_{photon} for ZnO–GeO_2 nanofibers prepared at 600, 700, and 800 °C. Intersections of the dashed lines with the abscissa represent the band-gap energies

Conclusion

In summary, we synthesized ZnO–GeO_2 nanofibers at temperatures in the range from 600 to 800 °C. Calcination of the nanofiber mats, produced by electrospinning a sol–gel consisting of zinc acetate dihydrate, germanium isopropoxide, and PVA in air at different temperatures for 1 h, completely eliminates the PVA polymer and decomposes the zinc acetate into ZnO and the germanium isopropoxide into GeO_2. The calcination temperature has a distinct effect on the nanofiber's average diameter and crystallinity. Smooth, compact, thin ZnO–GeO_2 nanofibers with good crystallinity are produced at a calcination temperature of 700 °C. The calcination temperature does not have a noticeable effect on the band gap energy difference of ZnO–GeO_2 nanofibers. Additionally, sharp and strong green emission peaks observed for room temperature PL spectra indicate that these synthesized nanofibers have good optical properties and are promising for the fabrication of efficient nano-optoelectronic devices in the near future.

Acknowledgements This study was supported by a grant from the Korean Ministry of Education, Science and Technology (The Regional Core Research Program/Center for Healthcare Technology & Development, Chonbuk National University, Jeonju 561-756 Republic of Korea). We thank Mr. T. S. Bae and J. C. Lim, KBSI, Jeonju branch, and Mr. Jong- Gyun Kang, Centre for University Research Facility, for taking the high-quality FE-SEM and TEM images, respectively.

References

1. Kanjwal MA, Barakat NAM, Sheikh FA, Khil MS, Kim HY (2008) J Mater Sci 43:5489. doi:10.1007/s10853-008-2835-3
2. Dai HQ, Gong J, Kim HY, Lee D (2002) Nanotechnology 13:674
3. Dharmaraj N, Kim CK, Prabu P, Ding B, Kim HY, Viswanathamurthi P (2007) Int J Electrospun Nanofibers Appl 1:63
4. Yuh JH, Nino JC, Sigmund WM (2005) Mater Lett 59:3645
5. Ju YW, Park JH, Jung HR, Choa SJ, Lee WJ (2008) Mater Sci Eng B 147:7
6. Peng XS, Meng GW, Wang XF, Wang YW, Zhang J, Liu X (2002) Chem Mater 14:4490
7. Zhou XF, Zhao Y, Cao X, Xue YF, Xu DP, Jiang L (2008) Mater Lett 62:470

8. Shaoa CL, Yua N, Liu YC, Mu RX (2006) J Phys Chem Solids 67:1423
9. Yu N, Shao CL, Liu YC, Guan HY, Yang XH (2005) J Colloid Interface Sci 285:163
10. Liping Z, Jiesheng L, Zhizhen Y, Haiping H, Xiaojun C, Binghui Z (2008) Opt Mater 31:237
11. Hiroyuki U (2007) J Phys Chem C 111:9060
12. Tang HP, Zhu LP, He HP, Ye ZZ, Zhang Y, Zhi MJ, Yang ZX, Zhao BH, Li TX (2006) J Phys D Appl Phys 39:2696
13. Chiu SJ, Lee MY, Chen HW, Chou WG, Lin LY (2002) Chem Biol Interact 141:211
14. Grossi V, Parisse P, Passacantando M, Santucci S, Impellizzeri G, Irrera A, Ottaviano L (2008) Appl Surf Sci 254:8093
15. Maeda Y, Tsukamoto N, Yazawa Y, Kanemitsu Y, Masumoto Y (1991) Appl Phys Lett 59:3168
16. Sadah JA, Tabet N, Salim M (2001) J Electron Spectrosc Relat Phenom 114:409
17. Jiang M, Wang Z, Ning Z (2009) Thin Solid Films 517:6717
18. Yu YS, Kim GY, Min BH, Kim SC (2004) J Eur Ceram Soc 24:1865
19. Zheng T, Li Z, Chen J, Shen K, Sun K (2006) Appl Surf Sci 252:8482
20. Zhang X, Chen Y, Jia C, Su Y, Li Q, liu L, Gou T, Wei M (2009) J Phys Chem C 113:13689
21. Leung YH, Djuris AB, Choy WCH, Xie MH, Gao J, Cheah KW, Man KYK, Chan WK (2005) J Cryst Growth 274:430
22. Li D, Xia YN (2004) Adv Mater 16:1151
23. Li D, McCann JT, Xia YN (2006) J Am Ceram Soc 89:1861
24. Greiner A, Wendorff JH (2007) Angew Chem Int Ed 46:5670
25. Viswanathamurthi P, Bhattarai N, Kim CK, Kim HY, Lee DR (2004) Inorg Chem Commun 7:679
26. Kanjwal MA, Barakat NAM, Sheikh FA, Khil MS, Kim HY (2009) Int J Appl Ceram Technol X:1
27. Formhals A (1934) US Patent 1,975,504
28. Yang Y, Chen H, Zhao B, Bao X (2004) J Cryst Growth 263:447
29. Lua L, Sahajwalla V, Kong C, Harris D (2001) Carbon 39:1821
30. Que W, Wang LL, Chen T, Sun Z, Hu X (2006) J Sol-Gel Sci Technol 38:147
31. Ballerini G, Ogle K, Labrousse MGB (2007) Appl Surf Sci 253:6860
32. Molle A, Bhuiyan MNK, Tallarida G, Fanciulli M (2006) Mater Sci Semicond Process 9:673
33. Umar A, Hahn YB (2006) Nanotechnology 17:2174
34. Djuri AB, Leung YH, Choy WCH, Cheah KW, Chan WK (2004) Appl Phys Lett 84:2635
35. Zhao L, Lian JS, Liu YH, Jiang Q (2008) Trans Nonferrous Met Soc China 18:145
36. Gu F, Wang SF, Lu MK, Zhou GJ, Xu D, Yuan DR (2004) J Phys Chem B 108:8119
37. Gu F, Wang SF, Lu MK, Cheng XF, Liu SW, Zhou GJ, Xu D, Yuan DR (2004) J Cryst Growth 262:182
38. Gu F, Li CZ, Hu YJ, Zhang L (2007) J Cryst Growth 304:369
39. Dare-Edwards MP, Goodenough JB, Hammett A, Trevellick PR (1983) J Chem Soc Faraday Trans 79:2027
40. Xu R, Zeng HC (2004) Langmuir 20:9780
41. Barakat NAM, Woo KD, Kanjwal MA, Kim HY (2008) Langmuir 24:11982